A novel eccentric lapping machine for finishing advanced ceramic balls

J. Kang and M. Hadfield

Bournemouth University, School of Design, Engineering & Computing,

Tribology Design Research Unit, Studland House, 12 Christchurch Road,

Bournemouth, Dorset, BH1 3NA, United Kingdom.

Email: jkang@bournemouth.ac.uk; mhadfiel@bournemouth.ac.uk

Abstract: Advanced ceramic balls are used extensively in hybrid precision ball bearings and show advantages in high speed, high temperature, high load and hostile environment. Finishing these balls with high quality, good efficiency and low cost is critical to their widespread application. A brief review on the methods of finishing ceramic balls is presented. The design of a novel eccentric lapping machine for finishing advanced ceramic balls is described. The kinematics of eccentric lapping is analysed and discussed, the symbolic expressions for the ball spin angular speed ω_b, ball spin angle β and ball circulation angular speed ω_c are derived and numerical solutions are plotted. Two kinds of HIPed (Hot Isostatically Pressed) silicon nitride ball blanks (13.25 mm ~ 13.50 mm in diameter) were lapped and polished to 12.700 mm using this machine. A maximum material removal rate of 68 μm per hour was achieved at the lapping step, which is much higher than by the traditional concentric lapping method. The polished ball surface roughness Ra value is 0.003 μm, and the ball roundness is 0.08~0.09μm which is above grade 5, and close to grade 3 of the precision bearing ball specification. This machine can be used as a prototype to develop a larger scale machine for production.

Keywords: lapping machine, finishing method, eccentric lapping, ceramic ball finishing, silicon nitride, hybrid bearings, ball lapping mechanism

NOTATION

R_b ball radius

R_g circular V-groove radius

R_i radius from the centre of the circular V-groove to the ball- V-groove inner contact point

R_o radius from the centre of the circular V-groove to the ball- V-groove outer contact point

r_i radius from rotating axis of lower lapping plate to ball- V-groove inner contact point

r_o radius from rotating axis of lower lapping plate to ball- V-groove outer contact point

E Eccentricity (the distance between rotating axis and centre of circular V-groove)

V_{ip} lower plate linear speed at ball /V-groove inner contact point perpendicular to the radial plane through centre of circular V-groove.

V_{op} lower plate linear speed at ball /V-groove outer contact point perpendicular to the radial plane through centre of circular V-groove.

θ ½ of V-groove angle

Ω_p lower lapping plate angular speed

ω_b ball spin angular speed

ω_c ball circulation around circular V-groove angular speed

1 INTRODUCTION

1.1 Background

Advanced ceramic balls should have the optimum combination of properties of low density, high elastic modulus, good corrosion resistance and temperature resistance for use as rolling elements in hybrid bearings (with steel inner and outer rings) and all-ceramic bearings [**1**]. The only restriction that prevents their widespread application is the high manufacturing cost of ceramic balls. The manufacturing processes of these ceramic elements can be classified into four stages, stage 1 – powder and fibre manufacture, stage 2 – green body forming, stage 3 – transformation to final shape, stage 4 – surface finishing [**2**]. Ceramic balls at stage 3 are made from processes of either Sinter + HIP (Hot Isostatic Pressing), or GPS (Gas

Pressure Sintering), or Direct HIP, or SRB (Sinter Reaction Bonding), or HP (Hot Pressing). In any case, a final surface finishing process is needed for the balls to achieve the required surface quality and geometric accuracy for precision ball bearing application. It is estimated that the surface finishing and associated inspection of ceramic balls for high contact stress applications constitutes about two thirds of the total cost of manufacturing. Therefore further extension of the application of advanced ceramic balls in hybrid bearings and all-ceramic bearings will depend on the development of cost effective finishing methods.

In industry, ceramic balls are typically finished by concentric lapping, using two plates placed face to face with matching concentric circular grooves on them, through several operations by gradually changing the load, plates and diamond grits sizes in the slurry or suspension. The ceramic ball surface skin produced in previous manufacturing stages which is compositionally and microstructurally different from the core of the ball has to be removed during the final finishing stage. For a 12.7mm ball, 500-800 μm stock in diameter has to be removed from the ball surface. It takes weeks to finish a batch of ceramic balls.

Obviously, the conventional finishing processes for ceramic balls need to be advanced. Some research has already been conducted in these areas. Magnetic Fluid Grinding (MFG), also called Magnetic Float Grinding (Polishing), was first developed by Tani and Kawata [**3**] and improved significantly using a float by Kato and Umehara [**4**]. Three research groups involved in Magnetic Fluid Grinding of ceramic balls are those of Kato [**5**], Childs [**6**] and Komanduri [**7**]. Storlaski etc. [**8,9**] using a four-ball rolling fatigue test machine as the grinding machine by replacing the upper ball with a stainless steel cone and the lower with 9 silicon nitride 6.5 mm diameter balls, studied the grinding wear of silicon nitride in diamond slurry at a relatively high speed (3,000 rpm or so). Fischer, etc. [**10**] studied the tribochemical polishing (TCP) of silicon nitride, a technique based on the friction-stimulated dissolution of material in a liquid with no abrasive particles. These researches provided some clues on advancing the finishing method of ceramic balls. If these laboratory-scale methods can be applied to production at large scale and at low cost, and if the ball roundness generated from these methods can reach the precision ball bearing requirements, are still unknown. In industry, the two plate lapping method is still the most common practice for finishing advanced ceramic balls. It is recognised that the fundamental mechanism of the loose abrasive process in the two plate method has received less attention and there is still great potential for further development.

1.2 Comparison of different two plate lapping mechanisms

1.2.1 Two flat surface lapping

Fig 1 shows the mechanism of two flat surface lapping. The balls being lapped are placed in between two flat lapping surfaces (upper disk and bottom disk) without any carrier separating the balls from each other. The top disk is stationary while the bottom disk is mounted on a planetary gear thus its motion consists of both self-rotation plus revolution around the spindle [**11**]. The balls being lapped are rolling and skidding in between the two plates, and their positions are changing at random. This mechanism can only be used for rough lapping.

1.2.2 One flat surface, loading tools and carrier lapping

Fig 2 portrays the mechanism of one flat surface, loading tools and carrier lapping. The lower lapping plate is a flat disk, while the upper one is called "tool", rotating and applying lapping pressure. Balls are separated by a carrier. If using a single tool, it will make a two point or three point contact of the ball according to the contact angle of the tool. Fig 2 (a) is a two point contact (contact angle = 180°), Fig 2 (b) is a three point contact. If two upper tools are used, that will make a four point contact (Fig 2 (c)), and two tools can apply a load independently [**11**].

1.2.3 One flat surface, one concentric V-groove lapping

Fig3 depicts the mechanism of one flat surface, one concentric v-groove lapping. The top lapping plate is a flat surface whilst the bottom plate has a circular V-groove on it. The centre of the circular V-groove is the rotational axis of the plate. Both top and bottom plates rotate independently along the same axis (Fig 3 upper). Balls being lapped are placed in the circular V-groove [**12**]. T. Kurobe etc. modified the lapping apparatus by separating the two sides of the V-groove into two parts (Fig 3 lower, B and C) which can rotate independently [**12,13**]. They designed a lapping apparatus in which the spin angle theta of finishing balls is controlled by changing the revolutionary speeds of the upper flat, outer half V-groove and inner half V-groove lapping plates (three plates can rotate independently). This lapping apparatus enables the spin angle theta of the ball to vary from 0° to 90°. It is found from experiments that the spin angle theta of the ball has a great influence on the lapping.

1.2.4 Two concentric circular groove lapping

Fig. 4 is a schematic of two concentric circular grooves lapping. Of the two lapping plates normally one is rotating and one is stationary, both with circular V-groove or round curve groove (conformal to the balls being lapped). The centre of the circular groove is the rotating axis. This is the most commonly used mechanism by industry to finish advanced ceramic balls.

1.2.5 One flat surface, one eccentric V-groove lapping

Fig 5 is a schematic of two plate eccentric lapping. The top plate with a flat lapping surface is stationary, while the lower plate with an eccentric V-groove on it is rotating. The distance between the centre of the circular V-groove and the rotating axis is the eccentricity. Such an eccentric lapping machine has been built up by the authors and found to be very promising in finishing advanced ceramic balls.

2 DESIGN OF A NOVEL ECCENTRIC LAPPING MACHINE

In order to investigate the loose abrasive process and the effects of different lapping parameters in the finishing of ceramic balls, an experimental eccentric lapping machine which allows finishing of 13.4 mm diameter ball blanks in a small batch (15 balls each time) was designed by the authors and manufactured in-house. Fig 6 is a picture of this machine. Fig 7 is its schematic.

A three-phase AC motor and gearbox combination (1) through pulleys and belt (2) drives flange shaft (3) to rotate at a pre-set speed. The speed of the AC motor is determined by the output current frequency of a Micro-Inverter (15). The input current frequency of the Micro-Inverter is 50 Hz, while the output current frequency of the Micro-Inverter can be set to 0.1 Hz ~ 400 Hz, which is the input of the AC motor. Because the input current frequency is proportional to the rotating speed of the AC motor, the rotating speed of the flange shaft can be set to 0.54 rpm ~ 2160 rpm. The lower plate (4) which has an eccentric V groove is mounted on the flange shaft. The top plate (6) which has a flat surface is stationary. Ceramic balls (5) are being lapped between the top plate and the V groove of the lower plate.

The lapping fluid outside the V groove circle on the lower lapping plate will flow to the hub of the flange shaft under centrifugal force and drip through a hole to the lapping fluid tray (8) underneath the flange shaft. From there the fluid goes through a pipe to the lapping fluid collection tank (7). Lapping fluid is pumped by a ProMinent gamma/4 diaphragm-type metering pump (11) at pre-set stroke through the

pipeline to the centre of top lapping plate. The lapping fluid is a mixture of diamond paste and lubricating fluid in a container (10) which is mixed and maintained in equal concentrations by a magnetic stirrer (9). The amount of lapping fluid applied is controlled by the pre-set stroke (number/min) of the pump and a timer. The applying time (i.e. 5 minutes) and time interval (i.e. every 3 hours) are controlled by this timer. During the timer's "On" period, the pump and magnetic stirrer will activate simultaneously. The load (lapping pressure) is applied to the top lapping plate by the spring loading unit (12). To ensure the lapping pressure is evenly distributed on all balls, the spring load is applied through a spherical element to the cone surface of a blind countersink on the top centre of the backing plate (13). A digital time counter (14) is connected to the voltage input of the AC motor, and the actual lapping time is counted.

Both top and lower lapping plates can be easily removed from the backing plate and flange shaft for change or trim. The lapping plates are made in pairs using different materials (cast iron, steel, and aluminium) and gives surface treatments. The eccentricity and angle of V groove also vary. To ensure the rotating speed of the lower plate is correctly set, a tachometer (SPM TAC10) is used by non-contact measurement, and the actual speed (r.p.m.) of the flange shaft is read digitally.

3 KINEMATICS OF ECCENTRIC LAPPING & DISCUSSION

In order to fully understand the eccentric lapping process and material removal mechanism, the analysis of ball kinematics is essential. In this section, some of the computations of symbolic expressions were carried out by Maple 6 software (Waterloo Maple Inc., Canada), and the numerical calculations and the plots were achieved in Microsoft Excel 97.

Fig. 8 shows the contact between a ball and the V-groove in lower plate. The radius from the centre of the circular V-groove to the ball/V-groove inner contact point, $R_{i,}$ is:

$$R_i = R_g - R_b \sin(\frac{\pi}{2} - \theta) = R_g - R_b \cos\theta \qquad (1)$$

The radius from the centre of the circular V-groove to the ball- V-groove outer contact point, R_o, is:

$$R_o = R_g + R_b \sin(\frac{\pi}{2} - \theta) = R_g + R_b \cos\theta \qquad (2)$$

Fig. 9 gives the geometric relationship between the ball/V-groove inner contact point, the ball/V-groove outer contact point and the lower plate rotation angle, which is in the section A-A of Fig.5. Presuming at time t=0, $r_i = R_i - E$, $r_o = R_o - E$, then at the instant of time t, the centre of the circular V-groove, the ball/V-groove inner contact point, and the centre of the rotating axis form the triangle $R_i\ r_i\ E$, and according to Cosine Rule from the triangle $R_i\ r_i\ E$,

$$R_i^2 = E^2 + r_i^2 - 2Er_i\cos(\pi - \Omega_p t) = E^2 + r_i^2 + 2Er_i\cos(\Omega_p t) \tag{3}$$

Equation (3) is a quadratic equation in r_i, and can be solved as:

$$r_{i1}, r_{i2} = -E\cos(\Omega_p t) \pm \sqrt{(E^2\cos(\Omega_p t)^2 + R_i^2 - E^2}$$

At $\Omega_p t = 0$, $r_i = R_i - E$, at $\Omega_p t = \pi$, $r_i = R_i + E$,

The real root is:

$$r_i = -E\cos(\Omega_p t) + \sqrt{(E^2\cos(\Omega_p t)^2 + R_i^2 - E^2} \tag{4}$$

According to the Sine Rule from the triangle $R_i\ r_i\ E$,

$$\frac{r_i}{\sin\alpha} = \frac{R_i}{\sin(\pi - \Omega_p t)} = \frac{E}{\sin\varphi}$$

$$\frac{r_i}{\sin\alpha} = \frac{R_i}{\sin(\Omega_p t)} = \frac{E}{\sin\varphi}$$

$$\sin\alpha = \frac{r_i}{R_i}\sin(\Omega_p t)$$

$$\alpha = \arcsin\left(\left(\frac{r_i}{R_i}\sin(\Omega_p t)\right)\right) \tag{5}$$

$$\sin\varphi = \frac{E}{R_i}\sin(\Omega_p t)$$

$$\varphi = \arcsin\left(\left(\frac{E}{R_i}\sin(\Omega_p t)\right)\right) \tag{6}$$

At time t, the centre of the circular V-groove, the ball/V-groove outer contact point, and the centre of the rotating axis form the triangle R_o r_o E, and according to the Cosine Rule from the triangle R_o r_o E,

$r_o^2 = R_o^2 + E^2 - 2ER_o\cos\alpha$

$$r_o = \sqrt{R_o^2 + E^2 - 2ER_o\cos\alpha} \tag{7}$$

Substituting α into equation (7) from equation (5), gives:

$$r_o = \sqrt{R_o^2 + E^2 - 2ER_o\sqrt{\frac{R_i^2 - r_i^2 + r_i^2\cos(\Omega_p t)^2}{R_i^2}}} \tag{8}$$

According to the Sine Rule from the triangle R_o r_o E,

$$\frac{r_o}{\sin\alpha} = \frac{E}{\sin\gamma}$$

$$\sin\gamma = \frac{E}{r_o}\sin\alpha = \frac{E}{r_o}\sin(\arcsin((\frac{r_i}{R_i}\sin(\Omega_p t))) = \frac{E}{r_o}\frac{r_i}{R_i}\sin(\Omega_p t)$$

$$\gamma = \arcsin(\frac{E}{r_o}\frac{r_i}{R_i}\sin(\Omega_p t)) \tag{9}$$

Fig.10 shows how the linear velocities on the lower plate at the ball/V-grove inner and outer contact points project perpendicular to the B-B plane (perpendicular to the radial plane through the centre of circular V-groove). The linear speed at the ball /V-groove inner contact point on the lower plate perpendicular to the radial plane through the centre of the circular V-groove, V_{ip}, is given by:

$$V_{ip} = r_i\Omega_p\cos\varphi = \Omega_p(-E\cos(\Omega_p t) + \sqrt{(E^2\cos(\Omega_p t)^2 + R_i^2 - E^2})\cos(\arcsin(\frac{E}{R_i}\sin(\Omega_p t)))$$

$$= \Omega_p(-E\cos(\Omega_p t) + \sqrt{(E^2\cos(\Omega_p t)^2 + R_i^2 - E^2})\sqrt{1 - \frac{E^2\sin(\Omega_p t)^2}{R_i^2}} \tag{10}$$

The linear speed at the ball /V-groove outer contact point on the lower plate perpendicular to the radial plane through the centre of the circular V-groove, $V_{op,}$ is:

$$V_{op} = r_o \Omega_p \cos\gamma = \Omega_p \sqrt{R_o^2 + E^2 - 2ER_o \sqrt{\frac{R_i^2 - r_i^2 + r_i^2 \cos(\Omega_p t)^2}{R_i^2}}} \cos(\arcsin(\frac{E}{r_o}\frac{r_i}{R_i}\sin(\Omega_p t)))$$

$$= \Omega_p \sqrt{R_o^2 + E^2 - 2ER_o \sqrt{\frac{R_i^2 - r_i^2 + r_i^2 \cos(\Omega_p t)^2}{R_i^2}}} \sqrt{1 - \frac{E^2 r_i^2 \sin(\Omega_p t)^2}{R_i^2 r_o^2}} \quad (11)$$

Fig.11, which is in the section B-B of Fig. 10, introduces the ball/V-groove, ball/top plate contact geometry and defines the independent ball kinematics variables — ball spin angular speed ω_b, ball spin angle β and ball circulation angular speed ω_c. In the analysis of ball kinematics, the following simplification has been made: the influence of occasional ball to ball contact is not included; the ball spin component normal to the plane of Fig. 11 is ignored which is equivalent to ignoring the gyroscopic effects (estimated to be small [**14**]); there is no sliding between ball and plates. In this case, at the ball/V-groove inner contact point,

$$V_{ip} = R_b \omega_b \cos(\frac{\pi}{2} - \theta + \beta) + R_g \omega_c \quad (12)$$

at the ball/V-groove outer contact point,

$$V_{op} = R_b \omega_b \cos(\theta - \beta) + R_g \omega_c \quad (13)$$

at the ball/top plate contact point,

$$0 = R_b \omega_b \cos\beta - R_g \omega_c \quad (14)$$

The three equations (12)~(14) with three unknown variables ω_b, ω_c and β, can be solved by eliminating ω_b, ω_c and β.

Subtract equation (13) from equation (12)

$$V_{ip} - V_{op} = R_b \omega_b \sin(\theta - \beta) - R_b \omega_b \cos(\theta - \beta) = R_b \omega_b (\sin(\theta - \beta) - \cos(\theta - \beta))$$

$$\omega_b = \frac{V_{ip} - V_{op}}{R_b(\sin(\theta - \beta) - \cos(\theta - \beta))} \quad (15)$$

From equation (14)

$$R_g \omega_c = R_b \omega_b \cos\beta \quad (14\text{-}1)$$

Substitute (14-1) into equation (12)

$$V_{ip} = R_b\omega_b \cos(\frac{\pi}{2} - \theta + \beta) + R_b\omega_b \cos\beta = R_b\omega_b(\sin(\theta - \beta) + \cos\beta) \quad (12\text{-}1)$$

Substitute ω_b into equation (12-1) with equation (15), and equation (12-1) becomes:

$$V_{ip} = \frac{(\sin(\theta - \beta) + \cos\beta)(V_{ip} - V_{op})}{\sin(\theta - \beta) + \cos(\theta - \beta)} \quad (12\text{-}2)$$

β can be derived from equation (12-2) as:

$$\beta = -\arctan\left[\frac{-V_{op} - V_{op}\sin(\theta) + \cos(\theta)V_{ip} + V_{ip}}{\cos(\theta)V_{op} + \sin(\theta)V_{ip}}\right] \quad (16)$$

Substitute β from equation (16), ω_b in equation (15) can be expressed as function of $\Omega_p t$.

From equation (14-1), substitute ω_b from equation (15)

$$\omega_c = \frac{R_b\omega_b \cos\beta}{R_g} = \frac{\cos\beta(V_{ip} - V_{op})}{R_g(\sin(\theta - \beta) - \cos(\theta - \beta))} = \frac{V_{ip}\sin(\theta) + V_{op}\cos(\theta)}{R_g(1 + \cos(\theta) + \sin(\theta))} \quad (17)$$

Fig. 12 shows the variations of ball spin angular speed ω_b, ball spin angle β and ball circulation angular speed ω_c at different contact points on the V-groove (designated as rotation angle of the lower plate) during a 360° rotation of the lower plate. This is under a typical lapping condition, R_b=6.5 mm, R_g=32.5mm, θ=45°, Ω_p=169 rpm =17.7 rad/s. The three curves are symmetric to 180°, this is in consistent with the eccentric V-groove geometry. The ball spin angular speed ω_b is in the range of 42.9~54.4 rad/s, which at first increases from the lowest to the highest as the lower plate rotation angle increases from 0° to 105°, then starts to decrease and maintains a relatively stable value around 51.8~53.4 rad/s and increases again as the lower plate rotation angle increases from 105° to 255° , and finally decreases from the highest to the lowest as the lower plate rotates from 255°to 360°. The ball spin angle β changes from 24.4°to –14.2°, a range of nearly 40°. This ball spin angle change is considered to be a beneficial to ball roundness as well as to material removal rate. The ball spin angle changes gradually as the lower plate rotation angle increases from 0° to 105°. From 105° to 180°, the ball spin angle change is sharp, and at 180° the direction is changed smoothly. From 180° to 360°, the ball spin angle change is symmetric with 180°~0°. The ball circulation angular speed ω_c is in the range of 7.8~10.4 rad/s, and the ball circulation direction is the same as the lower plate rotating direction. The value of ω_c increases gradually from 7.8~10.4 rad/s as the lower

plate rotates from 0° to 105°, maintains 10.4 rad/s unchanged from 105° to 255°, and decreases gradually to 7.8 rad/s from 255° to 360°. For both the ball spin angular speed ω_b, the ball spin angle β and the ball circulation angular speed ω_c, at the lower plate rotation angles105° and 255° are transition points. It is anticipated that at around these two points, micro-slip will occur, which will also be beneficial to ball roundness as well as to material removal rate. The ball circulation angular speed ω_c is 44%~59% of the lower plate angular speed Ω_p, depending on the relative location of the ball to the lower plate. For a specific ball, its location relative to the lower plate is changing by 56~41% of a full 360° revolution during each complete rotation of the lower plate, but this change could be different from one rotation to another. The ball angular spin speed ω_b and the ball spin angle β is changing all the time, which with the micro-slip between the ball and the plate at transition points, as well as the ball/plate contact, actually defines a Hertzian circular area of contact, so that all of the ball surface is lapped, and ball roundness is accurately achieved.

Fig. 13 demonstrates the influences of different eccentricity values (E =2, 4, 8, 12mm) on ball spin angular speed ω_b, ball spin angle β and ball circulation angular speed ω_c. All the other parameters remain unchanged as in Fig. 12, with R_b=6.5 mm, R_g=32.5mm, θ=45°, Ω_p=169 rpm =17.7 rad/s. As the eccentricity increases, the changing amplitudes of ω_b, β and ω_c are rising. Among the three variables, the extension of the changing amplitude of β is the most significant. At E=2mm, the changing amplitude of β is only about 10° while at E=12mm, the changing amplitude of β becomes 55°. The increase of the changing amplitude of ω_c is most insignificant, and for example at E=2mm, the ball circulation angular speed ω_c is almost a constant at the value ω_c=10.4 rad/s. The increase in the changing amplitude of the ball spin angular speed ω_b is associated with the changes in the transition points becoming more sharp. It also indicates that as the eccentricity increases, the transition points for ω_b, β and ω_c are shifting.

Fig. 14 illustates the influences of ½ V-groove angle θ on ball spin angular speed ω_b, ball spin angle β and ball circulation angular speed ω_c. The other parameters are set to be the same as in Fig. 12, i.e., R_b=6.5 mm, R_g=32.5mm, E=8mm, Ω_p=169 rpm =17.7 rad/s. The ½ V-groove angle θ does not affect ω_b and ω_c very much, with only a little sharpening at the transition points of ω_b as θ increases. The changing amplitude of β does not vary, although the angle of β is shifting.

Fig. 15 presents the influence of the lapping speed (Ω_p, specified as rpm for more straightforward understanding) on ball spin angular speed ω_b, ball spin angle β and ball circulation angular speed ω_c. All other parameters are the same as in Fig. 12, i.e., R_b=6.5 mm, R_g=32.5mm, E=8mm, θ=45°. The lapping speed has no effect on β, as the β value for all different lapping speeds are the same (the curves for β overlapped in Fig. 15). The ball spin angular speed ω_b is rising, whilst the change at transition points becomes sharper as the lapping speed is increasing. The ball circulation angular speed ω_c is rising proportionally as the lapping speed increases.

Fig. 16 reveals the influences of the circular V-groove radius R_g on ball spin angular speed ω_b, ball spin angle β and ball circulation angular speed ω_c. All other parameters are the same as in Fig. 12, i.e., R_b=6.5 mm, E=8mm, θ=45° and Ω_p=169 rpm =17.7 rad/s.. Comparing Fig. 16 with Fig. 13, for β and ω_c, the effects of increasing R_g are similar to decreasing E. For ball spin angular speed ω_b, this will rise proportionally with increasing R_g. So if R_g and E are increasing at the same time, probably β and ω_c will remain unchanged, but ω_b will rise. The increasing in ball spin angular speed ω_b will be beneficial for achieving better material removal rate and ball roundness, implying that even better lapping and polishing results could be achieved on a large scale eccentric lapping machine.

4 LAPPING AND POLISHING — RESULTS & DISCUSSION

4.1 Ceramic ball blanks

HIPed (Hot Isostatically Pressed) silicon nitride ball blanks, of high precision bearing ball material quality, were procured from two different manufacturers. The Ball Blanks from manufacturer A are designated as BBA, and Ball Blanks from manufacturer B are designated as BBB. Table 1 summarises some characteristics of these ball blanks. Surface hardness of these ball blanks was measured at load 10 kg, loading speed 100 μm/sec., load time 10 sec., using a Buehler machine. Ball blank surfaces were measured by a Zygo New View three dimensional imaging surface structure analyzer, Fig 17 are the 3D topographic images for BBA (Fig 17 (a)) and BBB (Fig 17 (b)) before finishing.

4.2 The influences of top and lower lapping plates

The material of the lapping plates could be critical to the performance of lapping and polishing. Cast iron, steel and aluminium have been utilised to make the top and lower plates (in pairs), and running the lapping and polishing tests. The experimental results show that the cast iron plates are appropriate in the first step of finishing —- lapping for achieving maximum material removal rate. Two types of cast iron material have been used, one being an ordinary, sand casting grade 12 grey cast iron. The maximum material removal rate has been achieved by using a pair of plates made from this type of cast iron. Another type of cast iron used is a continuous casting (grade 17 meehanite) cast iron which is assumed to have a more uniform and densified microstructure. The performance of this type of cast iron is still under investigation. Steel plates are suitable for the second step of finishing — polishing. Aluminium plates were worn very quickly after in service use, the anticipated diamond particle embedding in the plates and forming a hard, abrasive layer did not occur.

Besides the material of the plates, the conditions of the working surfaces of the lapping plates are directly related to the lapping and polishing results on the balls. It is found that the surface condition of the V-groove on the lower plate has a great influence on ball roundness and material removal rate, and that the surface state of the top plate is more influential on the final polished ball roughness.

4.3 Performance of lapping, the first step of finishing

The finishing process for advanced ceramic balls constitutes two steps: lapping and polishing. In the first step, maximum material removal rate is the goal while achieving fairly good ball roundness and maintaining no consequent ball surface and subsurface damage.

Taguchi Methods were used to optimise four lapping parameters—lapping load, lapping speed, diamond particle size and paste concentration to achieve maximum material removal rate and to evaluate the influence of each parameter on the material removal rate [**15**]. The analysis of variance (ANOVA) showed that the most significant lapping parameter was lapping load, which accounted for 50% of the total, followed by lapping speed (31%). The diamond particle size and paste concentration parameters only accounted for 12% and 7% respectively. Increasing the lapping load, lapping speed and paste concentration parameters causes a corresponding increase in material removal rate. The increase of material removal rate

is most significant as the lapping speed parameter increases from 118.42 rpm to 168.75 rpm. The increase of material removal rate is almost linear (proportional) with the increase of lapping load from average lapping load 0.9 kg/ball to 1.85 kg/ball.

An earlier study also shows that the increase of material removal rate is higher as the lapping speed changes from 8.5 rpm to79 rpm and from 140 rpm~169 rpm. The increase of material removal rate is lower as the speed increases from 79 rpm to 140 rpm. The interesting finding is that although the material removal rates of two kinds of ball blanks are very different, they increase proportionally as speed increases, BBA is always 3~4 fold of BBB at all different lapping speeds except at very low speed [**16**].

Recently, a high speed, high load aggressive lapping test has been conducted [**17**]. At first the material removal rate increased with the increase of lapping load reaching the maximum, 68μm/hour, at a load of 4.37kg/ball. At higher loads, the material removal rate decreased to 55μm/hour at a load of 6kg/ball, 25 μm/hour at 7.95kg/ball and 20 μm/hour at 10.87kg/ball. The increase of material removal rate with speed is not obvious within the speed range from 169 rpm to 500 rpm. A dye-penetrant, ultra-violet light microscopy inspection has been conducted after aggressive lapping to explore the possibility of surface or subsurface damage induced by finishing process. Surface spalls, subsurface star cracks and straight line area cracks were found on balls after lapping at 10.87kg/ball average load. No substantial surface or subsurface damage was found on balls after lapping at an average load of 4.37kg/ball. Surface spalls were found on balls after lapping at a speed of 500 rpm. No evidence of lapping induced surface damage, apart from C-cracks, was observed on balls lapped at 270 rpm. The radius of C-crack appears to be related to the lapping speed, but further work is needed to confirm this.

At the very early stage of the development of this eccentric lapping machine, a 4 mm eccentricity value E and a 120° V-groove angle (θ=60°) were used but found less satisfactory in material removal rate compared with 8 mm eccentricity and 90° V-groove angle. A 72 mm diameter circular V-groove (R_g=36mm) was used to accommodate 17 ball blanks but the lapping rate showed not as good as compared with a 65 mm diameter circular V-groove accommodating 15 ball blanks. At present, the systematic experimental investigation has not been completed on the influences of the eccentricity E, the ½ V-groove angle θ (also the symmetric axis of V-groove does not need to be parallel to rotating axis), and the radius of circular V-groove R_g. Furthermore, the comprehensive material removal mechanism is not fully explained

by the kinematic analysis alone, which concerns only the motion of the eccentric lapping. An attempt to establish a dynamic model, which involves both kinematic aspect, force, moment (torque), contact mechanics and loose abrasive particles scratching, is a present study. Both experimental and theoretical studies are needed in order to fully understand the eccentric lapping phenomena.

The maximum material removal rate achieved so far is under conditions of average lapping load 4.37kg/ball, lapping speed 169 rpm, diamond particle size 60 μm and diamond paste concentration 1g:30ml. The lapping machine parameters are: V-groove angle 90° (θ=45°) with symmetric axis parallel to rotating axis; the diameter of circular V-groove 65 mm (R_g=32.5mm); the eccentricity E 8 mm. A finishing rate of 68 μm/hour for ball blank BBA was achieved, which is 15 times higher than the conventional concentric lapping (normally 3~4μm/hour). A finishing rate of 18 μm/hour was achieved for ball blank BBB which is 10 times higher than the concentric lapping rate (normally 1~2μm/hour). The ball roundness at this step is 0.4~1.1 μm.

4.4 Performance of polishing, the second step of finishing

The second step in the finishing process is polishing, in which the ball surface roughness, roundness, dimensional and geometric accuracy are achieved. During polishing, the average load is from 1.1 kg/ball to 1.5 kg/ball, the speed is 94 rpm, and diamond particle sizes are 1 μm to ¼ μm. The polished ball surface roughness value Ra is 0.003 μm which is above grade 3 precision bearing ball specification, and ball roundness is 0.08~0.09μm which is above grade 5 and close to grade 3 precision bearing ball specification. Fig. 18 shows the surface profile data of a BBB ball after polishing analysed by a Zygo New View three dimensional imaging surface structure analyzer. Fig. 19 shows the roundness profile of a BBB ball after polishing using a Taylor-Hobson Talyrond 73 roundness profiler.

5 CONCLUSIONS

The lapping and polishing results of advanced ceramic balls on the novel eccentric lapping machine are superexcellent. Kinematic analysis reveals that the most influential parameters are the eccentricity E, the changing amplitudes of the ball spin angular speed ω_b, the ball spin angle β and the ball circulation angular speed ω_c which are increasing as E increases. The ½ V-groove angle θ has little effect. With an increasing in lapping speed, ω_b and ω_c rise proportionally but β remains unchanged. The effects of increasing circular V-groove radius R_g on β and ω_c are similar to decreasing E, but ω_b rises proportionally with increasing of R_g. This information can be used in designing a large scale eccentric lapping machine for production. Research is continuing with ongoing analysis of the mechanics of eccentric lapping involving both kinematics and dynamics including lapping pressure, friction force, centrifugal fore, lapping fluid drag force etc..

ACKNOWLEDGEMENTS

The authors would like to thank the financial support of the project from SKF Engineering & Research Centre B. V. in the Netherlands, in particular the technical advice from Dr Robin Cundill. Thanks are also due to F. J. Engineering in Milford on Sea, Hampshire (UK) for manufacturing the experimental lapping machine; to ProMinent Fluid Control (UK) Ltd, for contributing a Gamma/4 diaphragm-type metering pump; and to Dr Rahan Ahmed of Cambridge University (UK), Department of Engineering, for making measurements of the 3D topography of the balls.

REFERENCES

1 **Cundill, R. T.**, Light-weight material for the rolling elements of aircraft bearings, *Ball Bearing Journal,* 1983, **216,** 33-36.

2 **McColm, I. J.** and **Clark, N. J.**, *Forming, shaping, and working of high performance ceramics* 1988, Blackie and Son Ltd.

3 **Tani, Y.** and **Kawata, K.**, Development of High-Efficient Fine Finishing Process Using Magnetic Fluid, *CIRP Annals,* 1984, **33,** 217-220.

4 **Umehara, N.** and **Kato, K.**, Study on magnetic fluid grinding (1st report, The effect of the floating pad on removal rate of Si_3N_4 balls), *Nippon Kikai Gakkai Ronbunshu, C Hen/Transactions of the Japan Society of Mechanical Engineers, Part C,* 1988, **54,** 1599-1604.

5 **Umehara, N.** and **Kato, K.**, Magnetic fluid grinding of advanced ceramic balls, *Wear,* 1996, **200,** 148-153.

6 **Childs, T. H. C., Mahmood, S.** and **Yoon, H. J.**, Magnetic fluid grinding of ceramic balls, *Tribology International,* 1995, **28,** 341-348.

7 **Jiang, M.** and **Komanduri, R.**, On the finishing of Si3N4 balls for bearing applications, *Wear,* 1998, **215,** 267-278.

8 **Stolarski, T. A.** and **Jisheng, E.**, Effect of water in oil based slurry on wear of silicon nitride, *British Ceramic Transactions,* 1998, **97,** 61-67.

9 **Jisheng, E., Stolarski, T. A.** and **Gawne, D. T.**, Tribochemically assisted wear of silicon nitride ball, *Journal of the European Ceramic Society,* 1996, **16,** 25-34.

10 **Hah, S. R.** and **Fischer, T. E.**, Tribochemical polishing of silicon nitride, *Journal of the Electrochemical Society,*1998, **145,** 1708-1714.

11 **Ichikawa, S., Ona, H., Yoshimoto, I.** and **Kobayashi, A.**, Proposal of new lapping method for ceramic balls, *CIRP Annals,*1993, **42,** 421-424.

12 **Kurobe, T., Kakuta, H.** and **Onoda, M.**, Spin angle control lapping of balls (1st report) - theoretical analysis of lapping mechanism, *Seimitsu Kogaku Kaishi/Journal of the Japan Society for Precision Engineering,*1996, **62,** 1773-1777.

13 **Kurobe, T., Kakuta, H.** and **Onoda, M.**, Spin angle control lapping of balls (2nd report) - lapping of silicon nitride ball, *Seimitsu Kogaku Kaishi/Journal of the Japan Society for Precision Engineering,*1997, **63,** 726-730.

14 **Childs, T. H. C., Jones, D. A., Mahmood, S., Zhang, B., Kato, K.** and **Umehara, N.**, Magnetic Fluid Grinding Mechanics, *Wear* ,1994, **175,** 189-198.

15 **Kang, J.** and **Hadfield, M.**, Parameter optimization by Taguchi Methods for finishing advanced ceramic balls using a novel eccentric lapping machine, *Journal of Engineering Manufacture, Proceedings of Institution of Mechanical Engineer, Part B,* **accepted for publication in April 2000.**

16 **Kang, J.** and **Hadfield, M.**, A study on the lapping of ceramic ball, *Surface treatment IV -- computer methods and experimental measurements*, Assisi, Italy, Computational Mechanics Publications, Southampton, 1999, pp. 389-399.

17 **Kang, J., Cundill, R.** and **Hadfield, M.**, The consequences of aggressive lapping processes on the surface integrity of HIPed silicon nitride bearing balls, *Tribology in Environmental Design 2000,* Bournemouth, Professional Engineering Publishing Limited, London, UK, **In the press**.

LIST OF CAPTIONS FOR THE TABLES AND ILLUSTRATIONS

Table 1 Some characteristics of the two kinds of HIPed silicon nitride ball blanks tested

Fig. 1 Two flat surface lapping

Fig. 2 One flat surface, loading tools and carrier lapping

Fig. 3 One flat surface, one concentric V-groove lapping

Fig. 4 Two concentric circular grooves lapping

Fig. 5 One flat surface, one eccentric V-grooves lapping

Fig. 6 Overview of the novel eccentric lapping machine

Fig. 7 Schematic of the novel eccentric lapping machine

Fig. 8 Ball/V-groove inner and outer contact points

Fig. 9 Rotating speeds of lower plate at ball/V-groove inner and outer contact points

Fig. 10 Linear velocities at ball/V-groove inner and outer contact points projected to perpendicular to B-B plan

Fig. 11 Definition for ball kinematics variables

Fig. 12 The variations of ball spin angular speed ω_b, ball spin angle β and ball circulation angular speed ω_c during a 360° rotation of lower plate.

Fig. 13 Influences of eccentricity E on ball spin angular speed ω_b, ball spin angle β and ball circulation angular speed ω_c

Fig. 14 Influences of ½ V-groove angle on ball spin angular speed ω_b, ball spin angle β and ball circulation angular speed ω_c

Fig. 15 Influences of lapping speed on ball spin angular speed ω_b, ball spin angle β and ball circulation angular speed ω_c

Fig. 16 Influences of R_g on ball spin angular speed ω_b, ball spin angle β and ball circulation angular speed ω_c

Fig. 17 3D topographic imagines of ball blanks before finishing, (a) BBA, (b) BBB.

Fig. 18 3D surface profile of a ball after polishing

Fig. 19 The Talyrond roundness profile of a ball after polishing

	BBA (Ball Blank from manufacturer A)	BBB (Ball Blank from manufacturer B)
Manufacturing Process	directly HIPed , then rough ground	Sinter + HIPed
Density (kg/m^3)	3160	3237
Ball Diameter (mm)	13.255	13.46 ~ 13.50
Ball Roundness Variation (mm)	0.001	0.030 ~0.075
Surface Roughness Ra (μm)	0.202	2.645
Surface Hardness (Vikers Hardness Number)	1682	1532

Table 1 Some characteristics of the two kinds of HIPed silicon nitride ball blanks tested

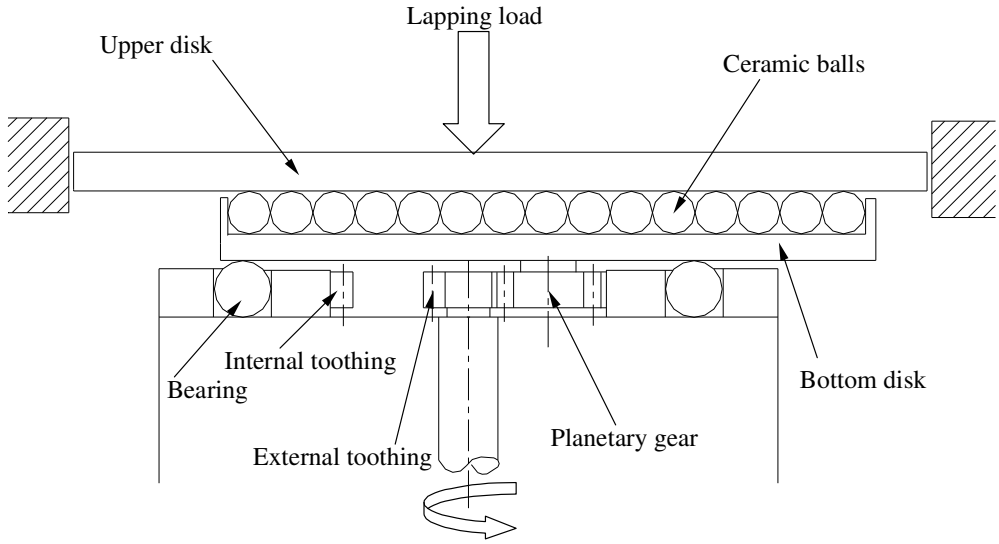

Fig.1 Two flat surface lapping

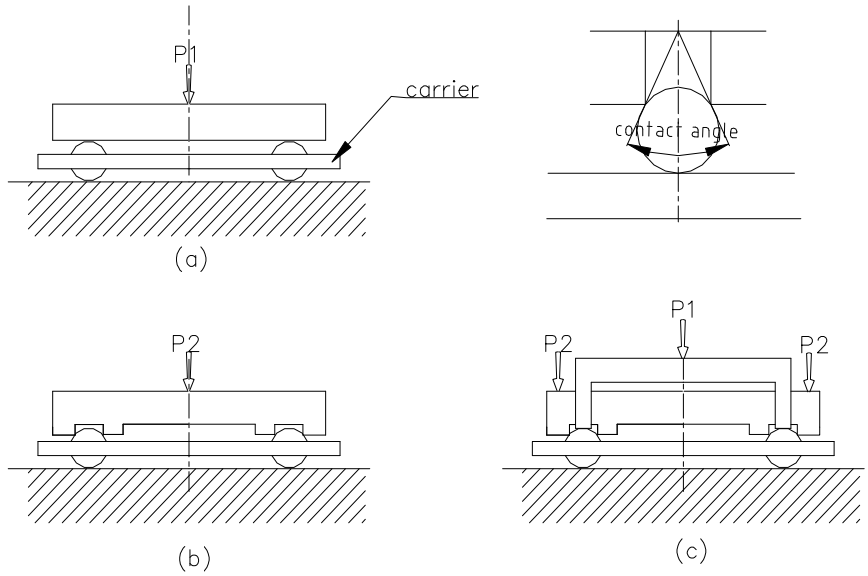

Fig. 2 One flat surface, loading tools and carrier lapping

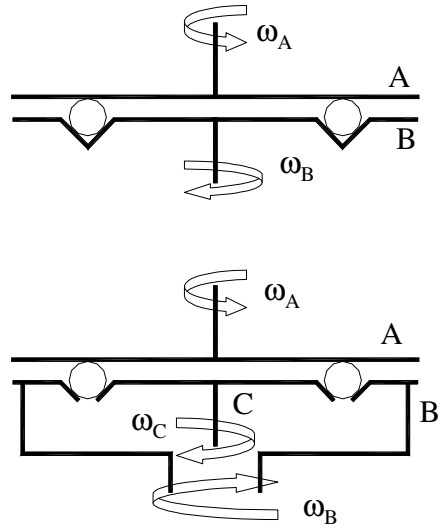

Fig. 3 One flat surface, one concentric V-groove lapping

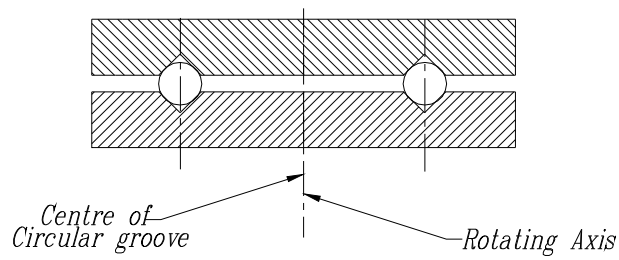

Fig. 4 Two concentric circular grooves lapping

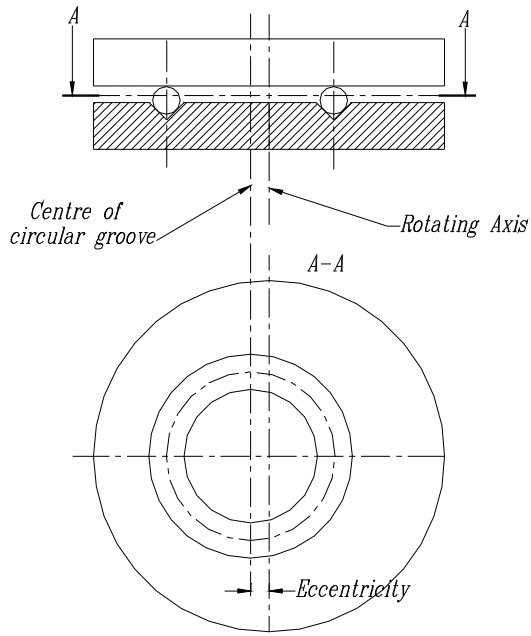

Fig. 5 One flat surface, one eccentric circular V-groove lapping

Fig. 6 Overview of the novel eccentric lapping machine

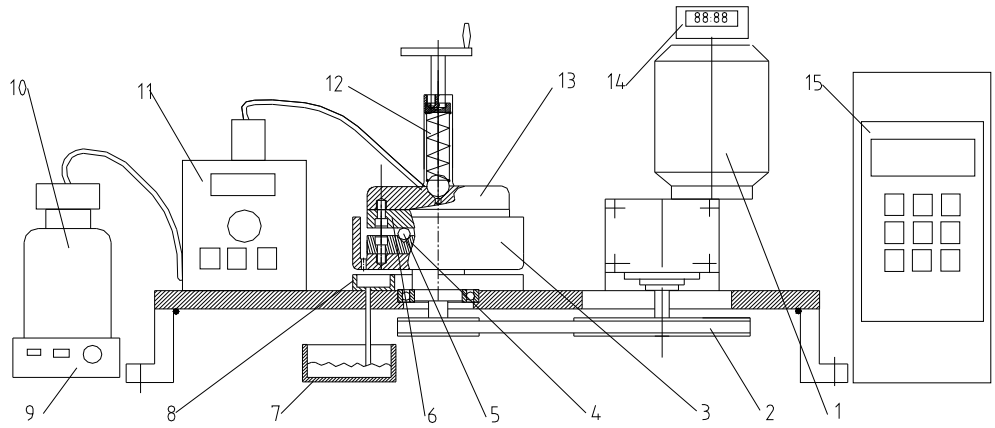

Fig. 7 Schematic of the novel eccentric lapping machine

1 AC motor and gearbox combination 2 Pulleys and belt 3 Flange shaft 4 Lower plate 5 Ceramic ball 6 Top plate 7 Lubricant fluid collection tank 8 Lubricant fluid tray 9 Magnetic stirrer 10 Lubricant fluid 11 Pump 12 Spring loading Unit 13 Backing plate 14 Time counter 15 Micro-Inverter

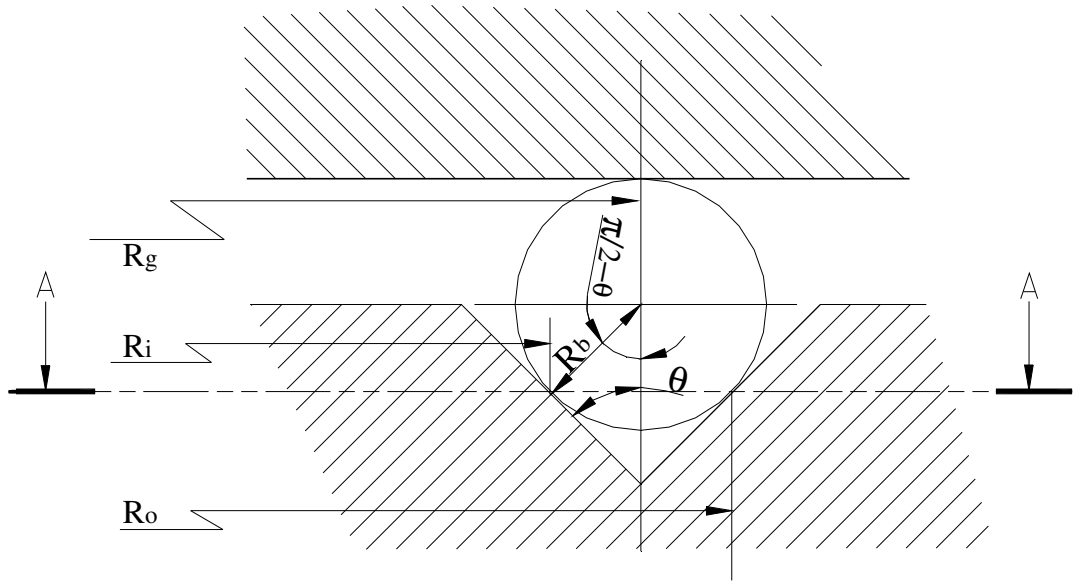

Fig. 8 Ball/V-groove inner and outer contact points

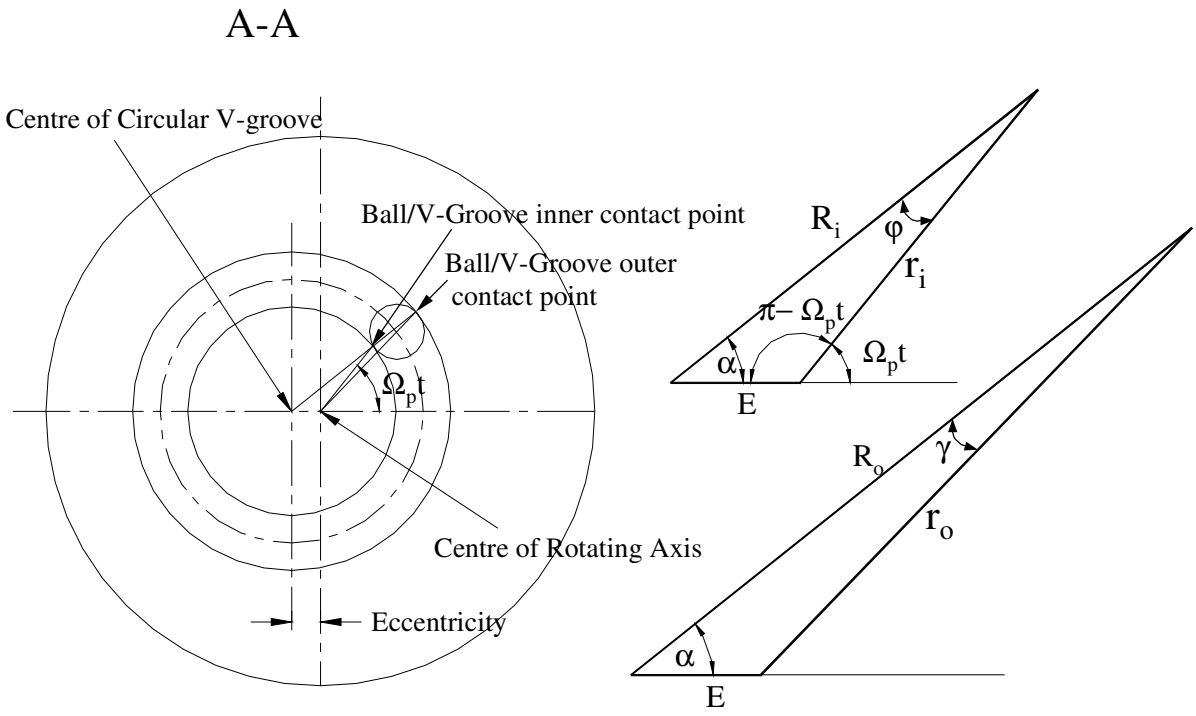

Fig. 9 Rotating speeds of lower plate at ball/V-groove inner and outer contact points

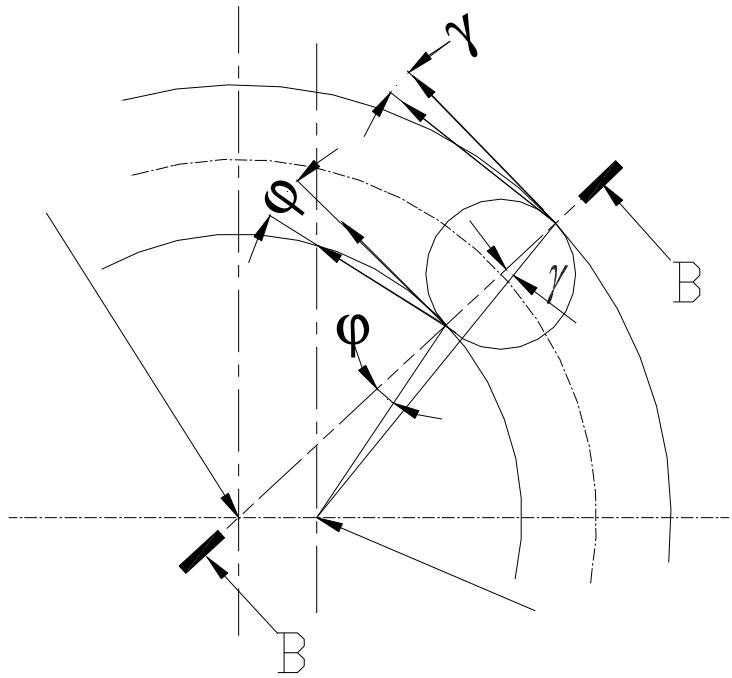

Fig. 10 Linear velocities at ball/V-groove inner and outer contact points projected to perpendicular to B-B plan

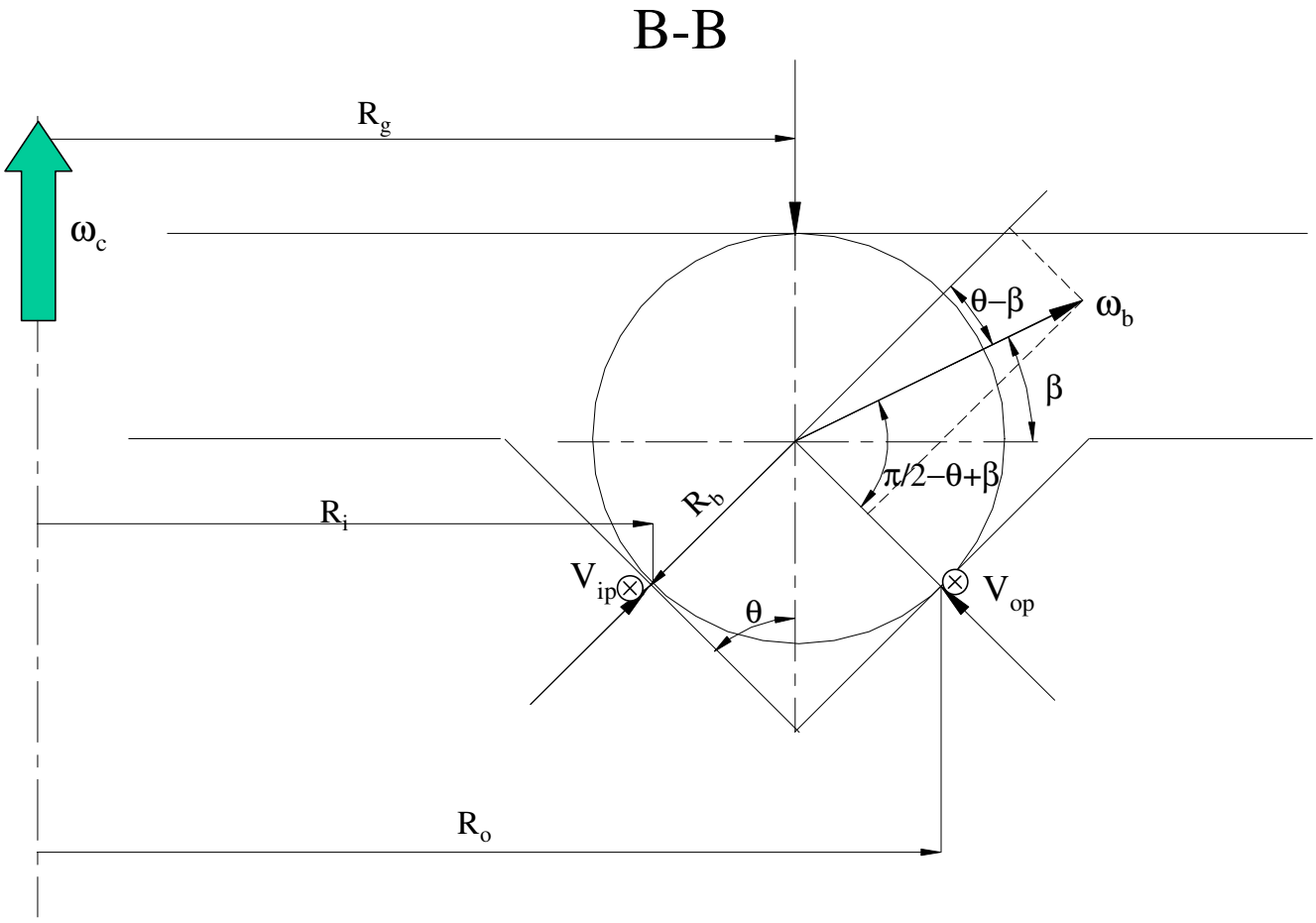

Fig. 11 Definition for ball kinematics variables

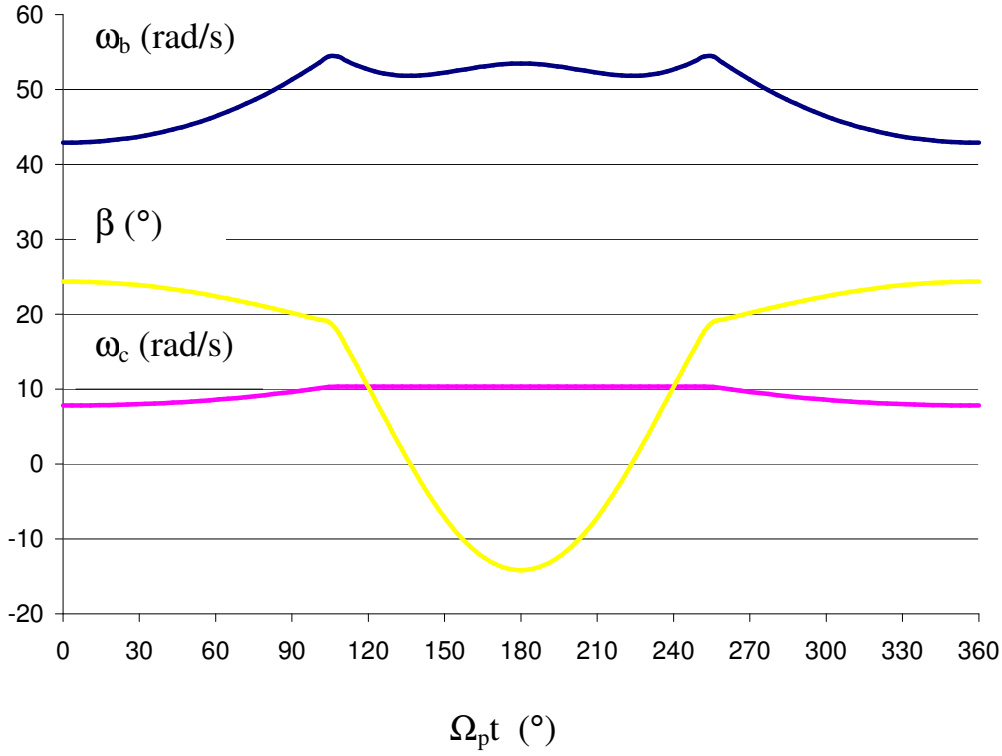

Fig. 12 The variations of ball spin angular speed ω_b, ball spin angle β and ball circulation angular speed ω_c during a 360° rotation of lower plate under a typical lapping condition.

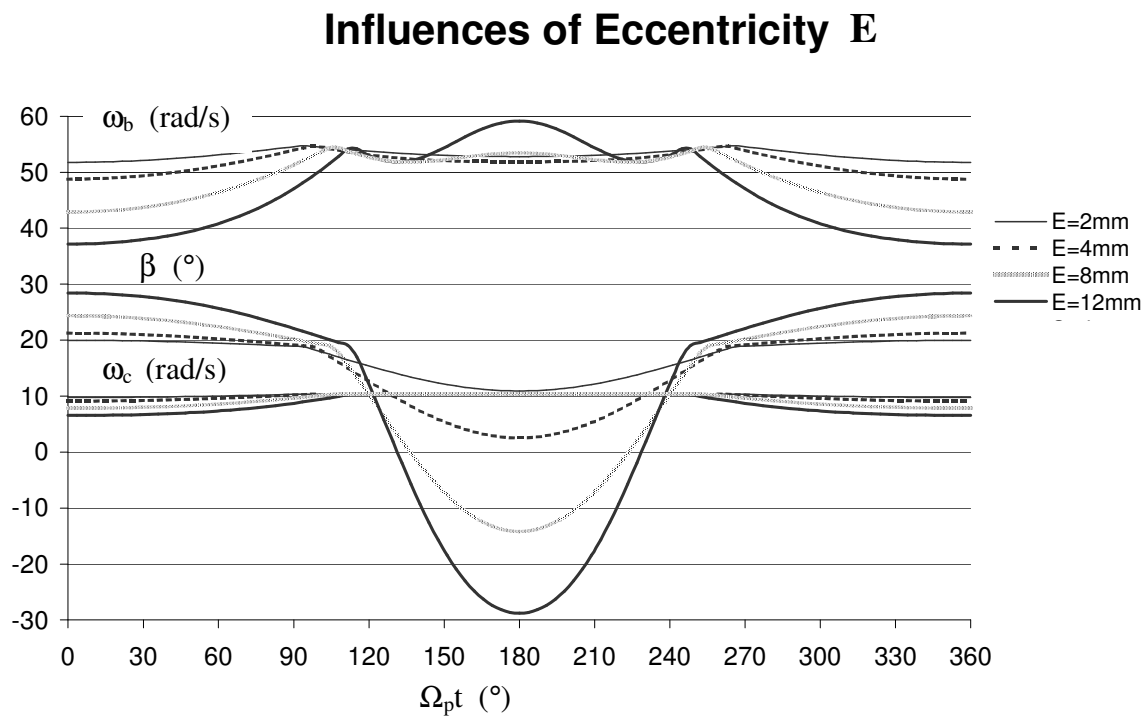

Fig. 13 Influences of eccentricity E on ball spin angular speed ω_b, ball spin angle β and ball circulation angular speed ω_c

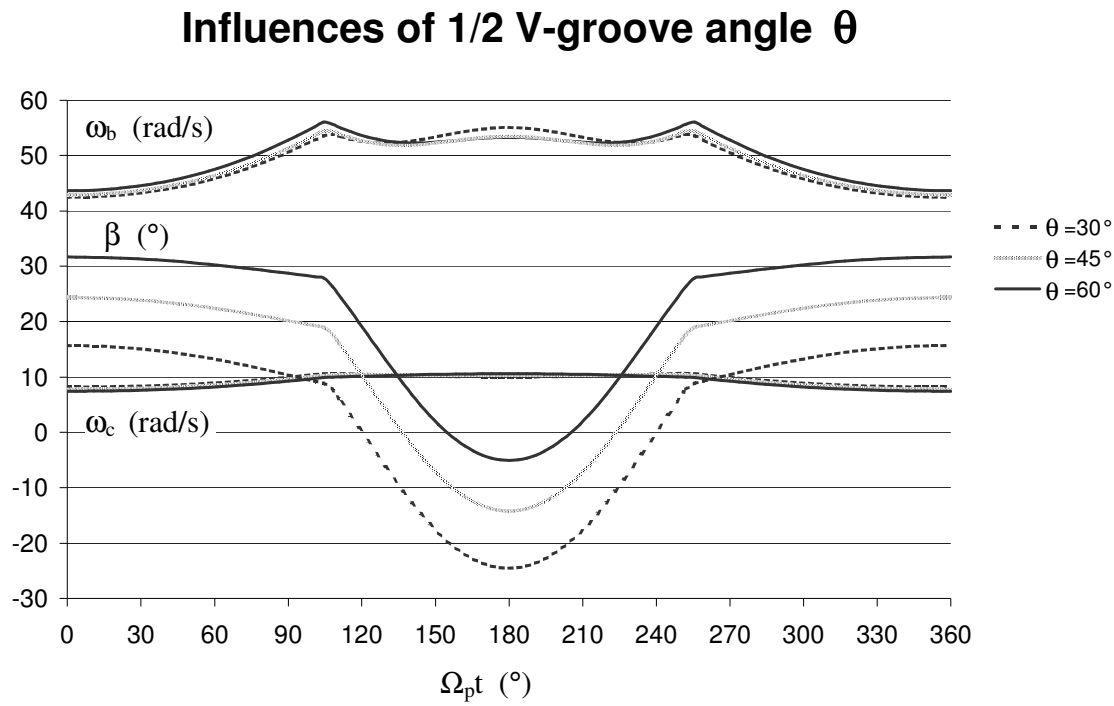

Fig. 14 Influences of ½ V-groove angle on ball spin angular speed ω_b, ball spin angle β and ball circulation angular speed ω_c

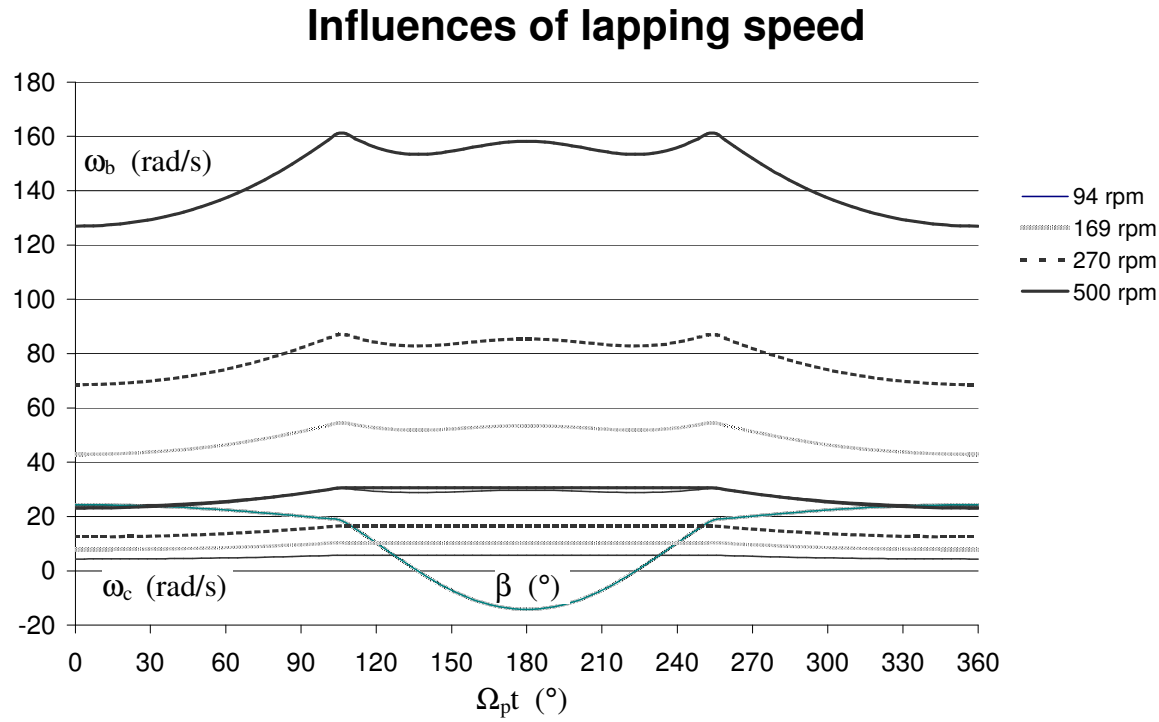

Fig. 15 Influences of lapping speed on ball spin angular speed ω_b, ball spin angle β and ball circulation angular speed ω_c

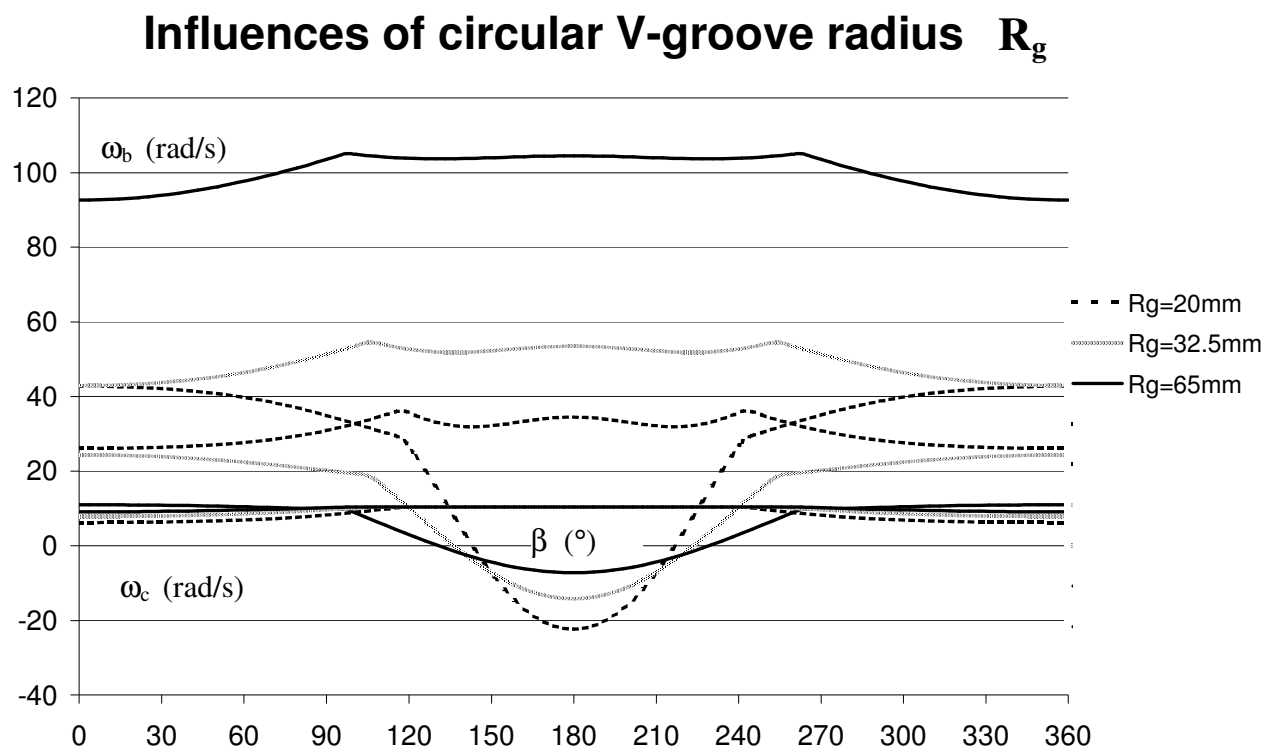

Fig. 16 Influences of circular V-grooove radius R_g on ball spin angular speed ω_b, ball spin angle β and ball circulation angular speed ω_c

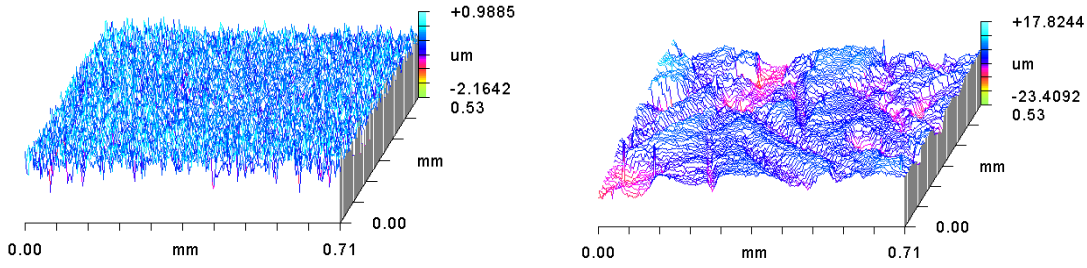

Fig. 17 3D topographic imagines of ball blanks before finishing, (a) BBA, (b) BBB.

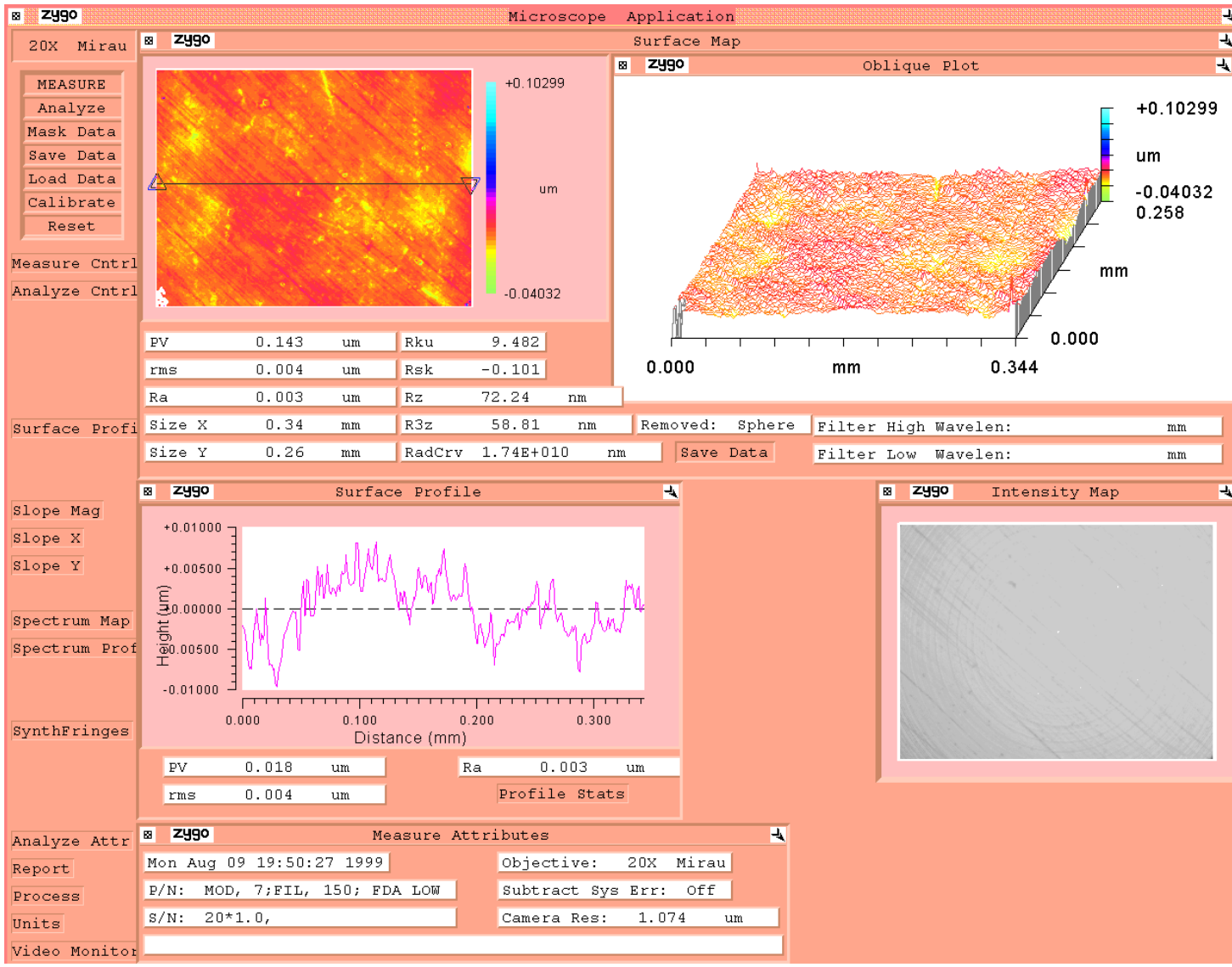

Fig. 18 3D surface profile of a ball after polishing

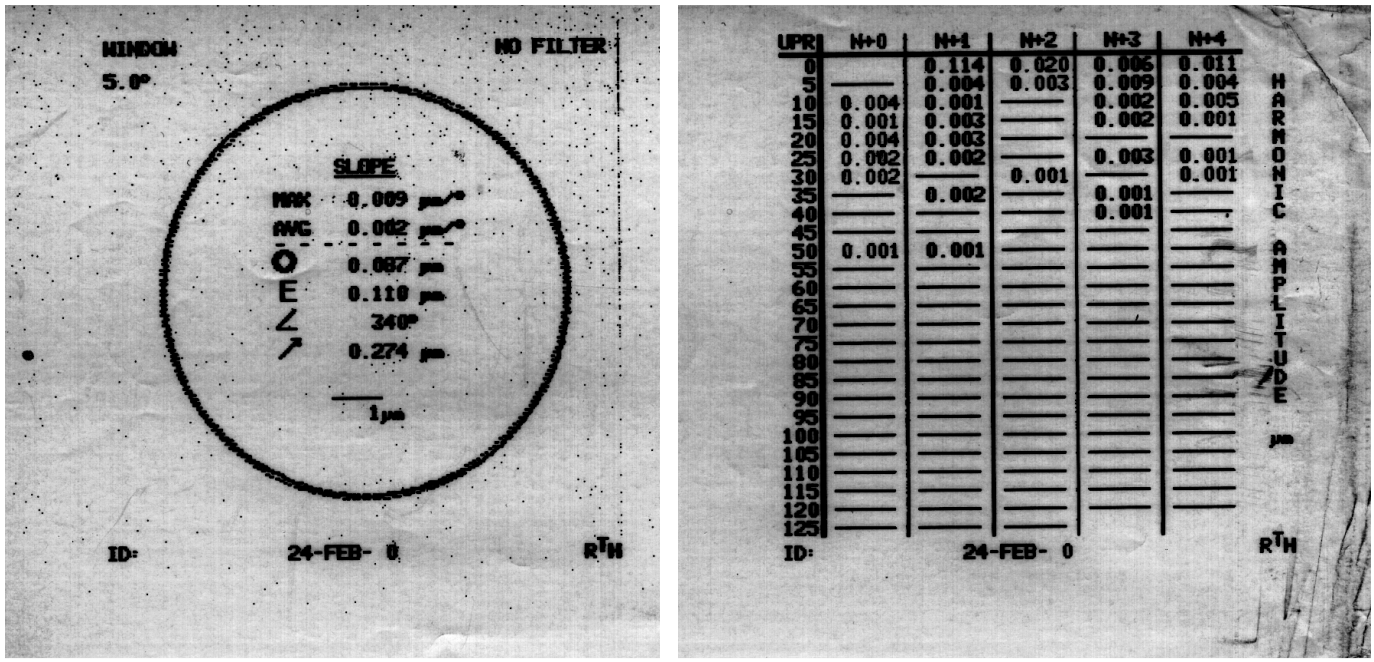

Fig. 19 The Talyrond roundness profile of a ball after polishing